

# Sub-5-fs two-dimensional spectroscopy of pseudoisocyanine J-aggregates

Kumiko Nishimura <sup>a</sup>, Eiji Tokunaga <sup>b</sup>, Takayoshi Kobayashi <sup>a,\*</sup>

<sup>a</sup> Department of Physics, Graduate School of Science, University of Tokyo, 7-3-1 Hongo, Bunkyo, Tokyo 113-0033, Japan

<sup>b</sup> Department of Physics, Faculty of Science, Tokyo University of Science, 1-3 Kagurazaka, Shinjuku, Tokyo 162-8601, Japan

Received 27 May 2004; in final form 5 July 2004

Available online 10 August 2004

## Abstract

The oscillations of the absorbance change due to molecular vibrations in pseudoisocyanine bromide J-aggregates were real-time resolved with sub-5-fs laser pulses. In spite of weak exciton–phonon coupling in the Frenkel exciton system, it was possible to observe the modulation of difference absorbance because of the enhanced transition moment. The non-Condon-type exciton–phonon coupling was invoked to explain the oscillatory signals and the transition dipole modulations were evaluated. The band at  $38\text{ cm}^{-1}$  was assigned to optical phonon mode, and the band at  $152\text{ cm}^{-1}$ , which had never been detected in Raman scattering, was also real-time resolved.

© 2004 Elsevier B.V. All rights reserved.

## 1. Introduction

J-aggregates of cyanine dye molecules have been extensively studied both experimentally and theoretically as a model material for one-dimensional Frenkel excitons [1–16]. One of the characteristic features of J-aggregates is the sharp excitonic absorption peak called the J-band, red-shifted from the monomer band [17,18]. Especially in the time domain, the dynamics of excitonic states have been observed with pulses of  $\approx 100$  fs in earlier investigations [19]. In the present letter, we utilized pulses as short as sub-5-fs for the pump–probe spectroscopy of J-aggregates of pseudoisocyanine bromide (PIC-Br) and detected impulsively excited coherent molecular vibrations in the aggregates for the first time. It has been difficult to observe the real-time oscillations, because the excitons in J-aggregates couple very weakly with the molecular vibration as confirmed by the small Stokes shift.

## 2. Experimental

The sample is a spin-coated thin film [20] of 1,1'-diethyl-2,2'-quinocyanine bromide, conventionally called pseudoisocyanine bromide (PIC-Br).

Femtosecond time-resolved pump–probe spectroscopy was performed at room temperature. The experimental setup was described previously [21,22]. In brief, the output 1-kHz pulse train from a noncollinear optical parametric amplifier [23,24] was chirp compensated and split into two beams for pump–probe spectroscopy in the range from 500 to 750 nm. The energy and the intensity of the pump pulse at the sample were  $\approx 40$  nJ and  $\approx 0.18\text{ GW/cm}^2$ , respectively. Weak pump–probe signals were detected with a multi-channel lock-in amplifier [25]. Real-time spectra were taken at delay times from  $-30$  to 2967 fs with a 3-fs step and its spectral range was from 553 to 597 nm.

Fig. 1a shows the stationary absorption (solid line) of PIC J-aggregates and the laser spectrum (dashed line). A sharp absorption peak centered around 575 nm is the J-band. In addition, there are two weaker peaks in the shorter wavelength side of the J-band, which can be as-

\* Corresponding author. Fax: +81 3 5841 41 65.

E-mail address: [kobayashi@femto.phys.s.u-tokyo.ac.jp](mailto:kobayashi@femto.phys.s.u-tokyo.ac.jp) (T. Kobayashi).

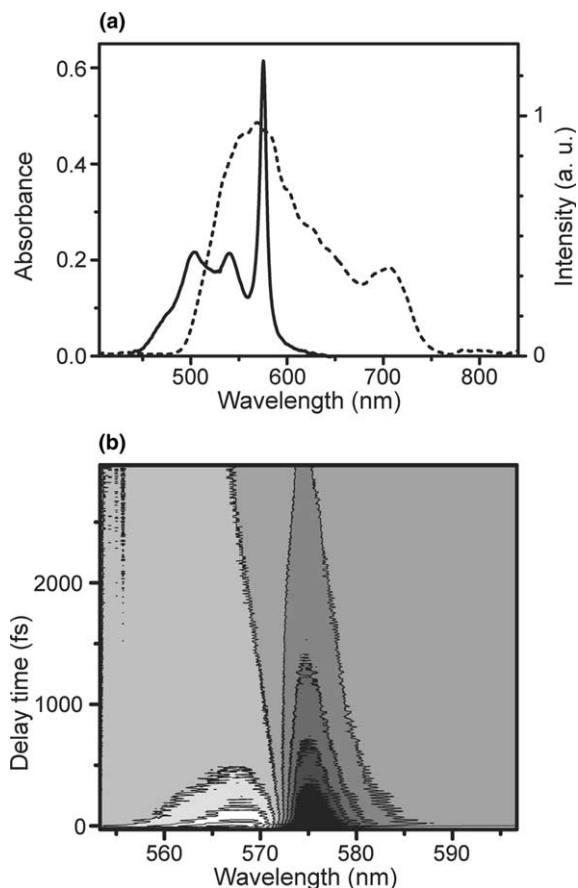


Fig. 1. (a) Stationary absorption (solid line) of PIC J-aggregates and the laser spectrum (dashed line). (b) Two-dimensional real-time spectrum in the time region from  $-30$  to  $2967$  fs and in the spectral region from  $553$  to  $597$  nm.

signed to the Davydov splitting components of the exciton band. This is confirmed from the fact that the peak wavelengths of the Davydov components differ from those of the monomer bands, indicating that most of the sample absorption is a contribution from J-aggregates.

### 3. Results and discussion

#### 3.1. Real-time difference transmission spectra

Fig. 1b shows a two-dimensional plot of the time-resolved difference absorption spectrum of PIC-Br J-aggregates. White – gray – black tones indicate positive (absorbance increase) and negative (absorbance decrease) changes. The spectral components shown in Fig. 2a can be decomposed into several contributions. The negative absorbance change ( $\Delta A$ ) around the peak of the J-band ( $575$  nm) is attributed to the bleaching (BL) due to the ground-state depletion and photo-induced emission (PIE) from the 1-exciton state. Because of the small Stokes shift, the BL and PIE signals being

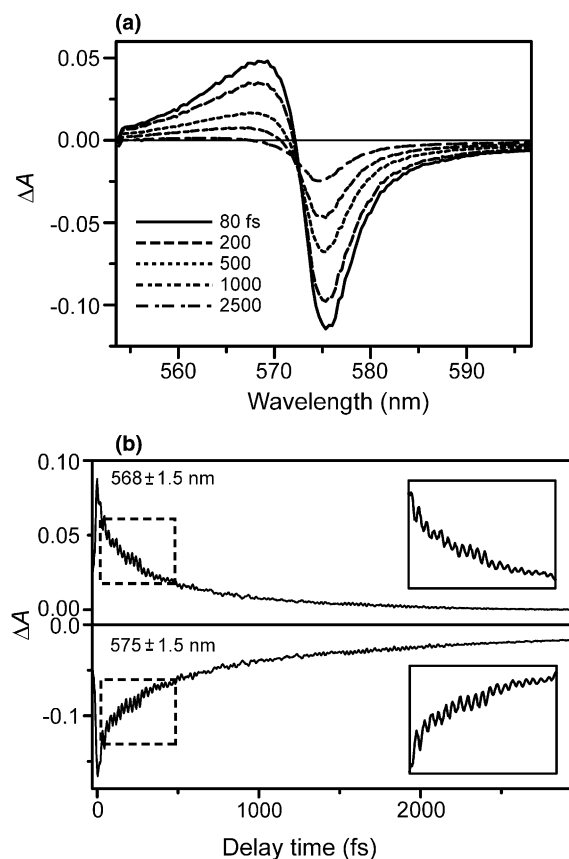


Fig. 2. (a) Averaged absorbance change spectra at delay times  $80$ ,  $200$ ,  $500$ ,  $1000$ ,  $2500$  fs over a  $60$ -fs interval. (b) Time traces integrated over  $3$ -nm ranges around IA (positive) and BL (negative) peak wavelengths. Inset shows enlargement of region surrounded by dashed box delay time from  $100$  to  $500$  fs.

overlapped, both signals contribute to the negative signal. The positive  $\Delta A$  around  $568$  nm is due to the induced absorption (IA) from the  $n$ - to  $(n+1)$ -exciton state [12,19],  $n$  being the number of excitons in a single mesoaggregate in which coherent exciton is delocalized over the mesoscopic size. The transition from 1-exciton state to 2-exciton state is expected to be predominant in a weak pump condition. In Fig. 2b, time traces integrated over  $3$ -nm ranges around IA (positive) and BL and PIE (negative) peak wavelengths are shown. In addition to a rapid decay of the multi-exciton state in which  $n$  delocalized excited-states exist, an oscillatory pattern is observed clearly from, as shown in the inset of Fig. 2b.

#### 3.2. FFT spectra and the origin of molecular vibration

To discuss the oscillatory signals, fast Fourier transformation (FFT) was performed on the real-time two-dimensional data for the delay times from  $150$  to  $2967$  fs. The resulting two-dimensional FFT power spectrum is depicted in Fig. 3 as a function of probe-wavelength (horizontal) and vibrational wavenumber (vertical).

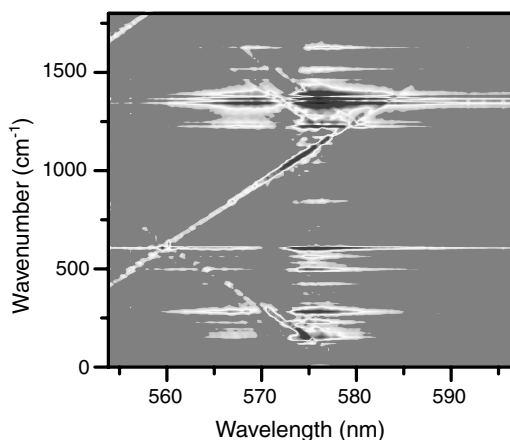


Fig. 3. Two-dimensional FFT power spectrum. Wavenumber resolution is  $\approx 10 \text{ cm}^{-1}$  determined by the condition of FFT.

There are also some oblique lines that are due to interference between scattered pump and probe light. Thanks to the two-dimensional spectrum, we can readily distinguish such false interference peaks from the real vibrational peaks.

### 3.2.1. FFT power spectra at typical probe-wavelength

Fig. 4a shows vertical slices at the two positive and negative peaks of BL and PIE (575 nm) and IA (568 nm). In both spectra, there are eleven prominent peaks at 152, 228, 282, 499, 607, 1225, 1247, 1344, 1366, 1388, and  $1626 \text{ cm}^{-1}$ . The insets show the enlarged spectra of three modes at 1344, 1366, and  $1388 \text{ cm}^{-1}$  in the dashed boxes, which are called triplet hereafter. The wavenumber resolution was limited to  $\approx 10 \text{ cm}^{-1}$ . The arrows show false FFT peaks resulting from the interference discussed above.

We will first discuss signals with  $>100 \text{ cm}^{-1}$ . From the wavenumbers these modes are considered to be due to intramolecular vibration. Akins et al. [26–28] measured stationary Raman scattering spectra of PIC monomers and J-aggregates. They assigned the low-wavenumber modes of 223 and  $278 \text{ cm}^{-1}$  to resonance- and aggregation-enhanced exciton–phonon modes. The major contribution to the  $223 \text{ cm}^{-1}$  Raman band is the twisting, while the bending is the predominant contribution to the  $278 \text{ cm}^{-1}$  band [28]. The vibrational modes in the present FFT spectra have the corresponding bands in the stationary Raman scattering spectra within  $\pm 7 \text{ cm}^{-1}$ , except for the band at  $152 \text{ cm}^{-1}$  (dotted circle). One can only tell that these corresponding bands coincide with the previous Raman data within the present wavenumber resolution of  $10 \text{ cm}^{-1}$ . The band at  $152 \text{ cm}^{-1}$  has never been observed because such a low-wavenumber mode is hardly detectable nor has it been predicted by calculation. Note that the  $152 \text{ cm}^{-1}$  band for probe-wavelength at 575 nm (Fig. 4a; right) is stronger because a false interference peak overlaps with the band. As for relative intensity, the present results differ

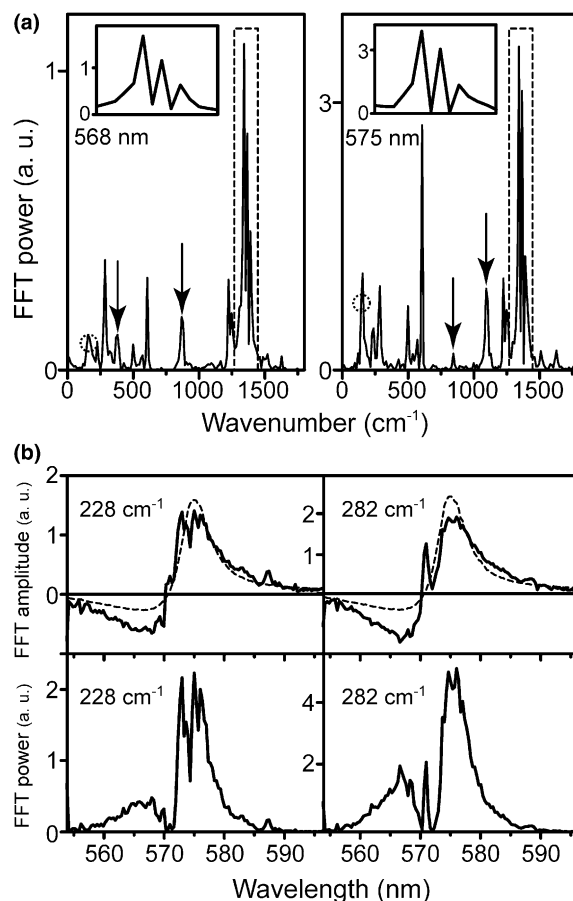


Fig. 4. (a) FFT power spectra of time trace at IA (left) and BL (right) peak wavelengths 568 and 575 nm, respectively. Inset is enlarged portion of dashed box and mode at  $152 \text{ cm}^{-1}$  is pointed by dotted circle. (b) FFT power spectra (bottom) of two low-wavenumber modes. FFT amplitude spectra (top, solid line) and the results of fittings (dashed line).

remarkably from those in the stationary Raman scattering spectra. First, the low-wavenumber modes at 228 and  $282 \text{ cm}^{-1}$  show less significant enhancement in the Raman scattering spectra. Second, the  $282 \text{ cm}^{-1}$  bands are much stronger than the  $228 \text{ cm}^{-1}$  bands while both bands have almost the same intensity in the Raman spectra. Third, for the triplet bands, the lowest band at  $1344 \text{ cm}^{-1}$  is the strongest in our FFT spectra while the middle band at  $1366 \text{ cm}^{-1}$  is the strongest in the Raman scattering spectra.

The main reason for these differences is that we have observed molecular vibration of spontaneous process in real-time measurement instead of stimulated process in Raman scattering measurement. We made a comparative study of the amplitude spectrum of the molecular vibrational modes excited impulsively by such 5-fs pulse and the Raman excitation profile (REP), and we showed several advantages of the former, which we called vibrational amplitude profile (VAP) over REP for the assignment of vibrational modes [29]. Another possible reason for these differences is that in the above-mentioned

Raman scattering experiments [26–28] both monomeric and aggregated PIC were adsorbed onto a metal surface, thus probably influenced by surface enhanced Raman scattering (SERS) effects. In addition, there are fundamental differences between the present real-time spectroscopy and conventional stationary Raman spectroscopy as follows. The spectrum of the present sub-5-fs pulsed source is so broad as to fully cover the exciton peak of PIC J-aggregates. This resonance condition is different from that of the stationary Raman scattering, in which an excitation laser is monochromatic and the degree of resonance depends on the laser wavelength. In the stationary Raman spectra the ground-state vibrations are detected, while in the FFT power spectrum of the real-time spectra wavepacket motions of both ground- and excited-states are detected, as will be discussed in the next subsection. Though electronic absorption and fluorescence spectra of the J-aggregate system lack vibrational progressions nearly completely because of exchange narrowing [6], we have now been able to observe such vibrationally coupled modes as many as eleven. This indicates the superiority of our ultrashort pulse multi-channel real-time spectroscopy for detection of the molecular vibration coupled to excitonic transition in such a system as J-aggregates.

Next, signals with  $<80\text{ cm}^{-1}$  are to be discussed. Fig. 5 shows the FFT power spectra at four probe-wavelengths for modes with  $<80\text{ cm}^{-1}$ , which do not appear

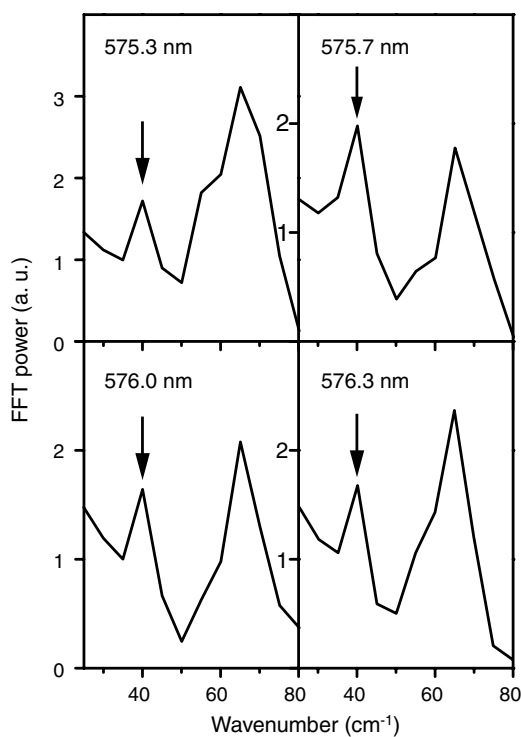


Fig. 5. FFT power spectra of four probe-wavelengths. The arrows indicate the positions of  $38\text{ cm}^{-1}$ .

in Fig. 4a because high-pass filtering was used to eliminate noise. Though the signal to noise ratios of the lower-frequency power spectra are not as good as those of higher-frequency modes shown in Fig. 4a, there are always two modes at  $38$  and  $65\text{ cm}^{-1}$  at almost all probe-wavelengths. The modes with  $65\text{ cm}^{-1}$  may be one of the bending modes of the whole PIC molecules, but it cannot be definitely assigned. The  $38\text{ cm}^{-1}$  mode can be assigned to the optical (lattice) phonon of the chain-structured J-aggregates, as discussed below. Kamalov et al. [15] discussed their experimental results of temperature dependence of relaxation in benzimidazolecarbocyanine (BIC)-aggregates in terms of temperature-assisted tunneling mediated with optical phonon with  $25\text{--}30\text{ cm}^{-1}$ . Since the molecular masses of BIC and PIC are  $779.5$  and  $327.4\text{ U}$ , respectively, the wavenumbers of optical phonon can be calculated for PIC to be  $39\text{--}46\text{ cm}^{-1}$  from the relation,

$$\frac{\omega_{\text{PIC}}}{\omega_{\text{BIC}}} = \sqrt{\frac{m_{\text{BIC}}}{m_{\text{PIC}}}} \quad (1)$$

The wavenumber of  $38\text{ cm}^{-1}$  then agrees well with the previous work [15]. Therefore, we have observed directly the intermolecular vibration in lattice phonon, which was previously expected only indirectly.

### 3.2.2. FFT amplitude dependences on probe-wavelength

Fig. 4b shows the FFT amplitude (top) and power (bottom) spectra of modulation signals due to the molecular vibrational wavenumbers with  $228$  and  $282\text{ cm}^{-1}$ . It is well established from previous studies including our own works that the negative  $\Delta A$  signal results from BL and PIE [19]. This implies that the wavepacket motions of both the ground- and 1-exciton states contribute to the FFT power in the corresponding spectral regions. On the other hand, in the spectral range where  $\Delta A$  is positive the oscillatory signal is considered to be mainly due to contribution of the IA. In the negative  $\Delta A$  side the relative amplitudes are larger than in the positive side with respect to those of absorbance change. This is probably due to the above-mentioned fact that the relative sizes of contributions to the amplitudes signals from the wavepackets of the exciton and ground-states are different between the positive and negative signal regions, but a further detailed study is needed to clarify the mechanism of this difference.

If we apply the conventional Franck–Condon-type wavepacket model to explain the origin of this molecular vibration, the integrated FFT amplitude in the whole spectral region of IA is expected to be constant [30]. However, since coherent oscillation is found to be present even in the integrated amplitude (data not shown), it cannot be explained in terms of the Franck–Condon-type wavepacket model. This kind of phenomenon in porphyrin J-aggregates was explained by non-Condon-type

dynamic intensity borrowing of a partially allowed Q-band from an allowed B-band [30].

### 3.3. Evaluation of the amount of modulated transition dipole moment

The fraction of the variation in the transition dipole moment due to molecular vibration is expressed as  $\delta\mu/\mu$ , where  $\mu$  and  $\delta\mu$  represent the transition dipole moment from the ground-state to the 1-exciton state and its variation, respectively. The intermolecular dipole–dipole interaction,  $J$ , is also modulated through this modulation  $\delta\mu$ . It is assumed for simplicity that all the transition dipoles are arranged parallel at angle  $\theta$  with the aggregate axis and the molecules are equidistant from their neighbors with a lattice constant  $a$ . Then  $J$  is given by,

$$J = \frac{\mu^2(1 - 3\cos^2\theta)}{\hbar a^3}. \quad (2)$$

The fraction of the coupling is given by the following equation in terms of the modulations of transition dipole moment,  $\delta\mu$ , and orientation angle,  $\delta\theta$ , as follows:

$$\frac{\delta J}{J} = \frac{2\delta\mu}{\mu} + \frac{3\sin(2\theta)}{3\cos^2\theta - 1} \delta\theta - \frac{3}{a} \delta a. \quad (3)$$

The modulation of  $J$  gives rise to a modulated peak photon frequency of the J-band in the transient absorption spectrum. The nonlinear spectrum,  $S_{\text{NL}}(\omega)$ , is phenomenologically assumed to be modified to  $S'_{\text{NL}}(\omega)$ , which is defined by the amounts of  $\delta\mu$  and  $\delta(2J)$  as follows:

$$S'_{\text{NL}}(\omega) = S_{\text{NL}}(\omega - \delta\omega(t))(1 + \delta\alpha(t)). \quad (4)$$

Here the time-dependent absorbance modulation  $\delta\alpha(t)$  and frequency modulation  $\delta\omega(t)$  are expressed as,

$$\delta\alpha(t) = \delta\alpha \cos(\Omega t) \equiv (\delta(\mu^2)/\mu^2) \cos(\Omega t), \quad (5)$$

$$\delta\omega(t) = \delta\omega \cos(\Omega t) \equiv \delta(2J) \cos(\Omega t), \quad (6)$$

where  $\delta\alpha$  and  $\delta\omega$  correspond to the modulated amplitude and frequency, respectively, of the pump–probe spectrum. The modulation frequency,  $\omega$ , corresponds to each vibrational mode. The equation can be approximated as,

$$\begin{aligned} S'_{\text{NL}}(\omega) &\cong S_{\text{NL}}(\omega) + \left( \delta\alpha S_{\text{NL}}(\omega) - \delta\omega \frac{dS_{\text{NL}}(\omega)}{d\omega} \right) \cos(\Omega t) \\ &\equiv S_{\text{slow}}(\omega) + S_{\text{osc}}(\omega) \cos(\Omega t). \end{aligned} \quad (7)$$

The nonlinear spectrum,  $S_{\text{NL}}(\omega)$ , consists of the slow-dynamics component ( $S_{\text{slow}}(\omega)$ ) and the oscillating component ( $S_{\text{osc}}(\omega)$ ).  $S_{\text{osc}}(\omega)$  corresponds to the FFT amplitude as a function of probe-frequency. From the fitting coefficients  $\delta\alpha$  and  $\delta\omega$ , we can estimate both  $\delta\mu/\mu$  and  $\delta(2J)$ . The real-time spectrum used to fit the FFT amplitude spectrum was obtained by averaging  $\Delta A$  spectra in the time region from 150 to 2967 fs. The two spectra at the top of Fig. 4b show the results of

the least-squares fitting (dashed line) of two low-wavenumber modes (solid line). Each FFT amplitude spectrum was well fitted only with the  $S_{\text{NL}}(\omega)$  spectrum without the  $dS_{\text{NL}}(\omega)/d\omega$  spectrum. From this analysis the  $\delta\mu/\mu$  for 228 and 282  $\text{cm}^{-1}$  were estimated to be about 0.3% and 0.5%, respectively. One of the possible explanations for the absence of  $dS_{\text{NL}}(\omega)/d\omega$  contribution in the fit is an accidental cancellation of the modulation by the synchronous modulation of the ground-state crystal shift. Another possible explanation is the accidental cancellation of the modulation by that of  $\delta\theta$  or  $\delta\alpha$  in case they have opposite sign to that of  $\delta\mu$ . At this stage it is difficult to identify the origin of the negligible contribution of  $dS_{\text{NL}}(\omega)/d\omega$  and needs a further study to clarify it.

The fitting curves for both 228 and 282  $\text{cm}^{-1}$  are smaller than the FFT amplitude curves. This can be explained in the following way.

In the range of wavelength longer than 570 nm, the  $\Delta A$  signal is due both to the BL and PIE. In both processes, wavepackets on the ground- and excited-states can both contribute to the modulation. In the range shorter than 570 nm, on the other hand, the  $\Delta A$  signal is dominantly due to IA. If the four contributions in the longer spectral range, namely the ground-state wavepacket to the BL and PIE and the excited-state wavepacket to the BL and PIE, interfere destructively, then the relative sizes of modulation in that region can be smaller than those in the shorter wavelength region. There is another possible explanation of the smaller FFT amplitude in the longer wavelength. IA can have a contribution from the transition other than 1- to 2-exciton state, namely to the excited exciton. In this case the characteristic property of the ground-state-to-1-exciton transition can be quite different from 1-exciton-to-excited exciton transition. Then the vibronic coupling strengths of the two transitions can be quite different.

The Frenkel exciton system is well-known to have very weak exciton–phonon coupling. In the present study, we have observed the real-time exciton–phonon coupling, which has resulted in the modulation of electronic transitions associated with the BL, PIE, and IA. This is because of the enhanced transition probability, which is proportional to  $N\mu^2$ ,  $N$  being number of molecules in the mesoaggregate [31]. In the PIC J-aggregates,  $N$  was estimated to be  $\approx 55$ . The transition probability is hence enhanced by  $\approx 55$ , and any weak exciton–phonon coupling can induce a detectable change as large as  $N\delta\mu$ .

## 4. Conclusion

We have observed real-time coherent oscillations due to the vibrational modes in PIC J-aggregates. Eleven vibrational modes are extracted from two-dimensional FFT of the real-time data. The two-dimensional spectra are utilized to exclude false peaks caused by the interfer-

ence between the scattered pump and the probe. We have detected motions of the wavepackets both in the ground- and 1-exciton states separately according to their wavelength range. The vibrational mode of  $152\text{ cm}^{-1}$  has never been detected in conventional measurements of Raman scattering. The other ten modes agree with the Raman data within  $\pm 7\text{ cm}^{-1}$ ; this indicates the range of vibrational energy differences of these states. On the other hand, the relative intensities of these modes differ from those in the Raman scattering data because of difference in the experimental conditions. We have directly observed intermolecular vibration in lattice phonon coupled to the excitonic transition in J-aggregates. We have further applied the non-Condon-type exciton-phonon coupling in the J-aggregates to explain the oscillatory signals and evaluated  $\delta\mu/\mu$  for the vibrational modes of  $228$  and  $282\text{ cm}^{-1}$  to be about  $0.3\%$  and  $0.5\%$ , respectively.

### Acknowledgements

The authors are grateful to Drs. H. Kano and N. Fukutake for fruitful discussions. This research is supported partly by the Grant-in-Aid for Specially Promoted Research (#14002003) from the Ministry of Education, Science and Culture and also partly by the program for the Promotion of Leading Researches in Special Coordination Funds for Promoting Science and Technology from the Ministry of Education, Science and Culture.

### References

- [1] T. Kobayashi (Ed.), J-aggregates, World Scientific, Singapore, 1996.
- [2] C.G. Granqvist, O. Hunderi, Phys. Rev. 16 (1977) 3513.
- [3] B. Kopainsky, W. Kaiser, Chem. Phys. Lett. 88 (1982) 357.
- [4] B. Kopainsky, J.K. Hallermeier, W. Kaiser, Chem. Phys. Lett. 87 (1982) 7.
- [5] P.O.J. Scherer, S.F. Fischer, Chem. Phys. 86 (1984) 269.
- [6] E.W. Knapp, Chem. Phys. 85 (1984) 73.
- [7] Y. Wang, Chem. Phys. Lett. 126 (1986) 209.
- [8] V. Sundström, T. Gillbro, R.A. Gadonas, A. Piskarskas, J. Chem. Phys. 89 (1988) 2754.
- [9] F.C. Spano, S. Mukamel, Phys. Rev. A 40 (1989) 5783.
- [10] H. Fidler, J. Terpstra, D.A. Wiersma, J. Chem. Phys. 94 (1991) 6895.
- [11] J. Knoester, J. Chem. Phys. 99 (1993) 8466.
- [12] H. Fidler, J. Knoester, D.A. Wiersma, J. Chem. Phys. 98 (1993) 6564.
- [13] S. Kobayashi, F. Sasaki, Nonlinear Opt. 4 (1993) 305.
- [14] K. Misawa, K. Minoshima, T. Kobayashi, J. Raman Spectrosc. 26 (1995) 553.
- [15] V.F. Kamalov, I.A. Struganova, K. Yoshihara, J. Phys. Chem. 100 (1996) 8640.
- [16] N. Fukutake, T. Kobayashi, Chem. Phys. Lett. 356 (2002) 368.
- [17] E.E. Jelly, Nature 138 (1936) 1009.
- [18] G. Scheibe, Angew. Chem. 49 (1936) 563.
- [19] K. Minoshima, M. Taiji, K. Misawa, T. Kobayashi, Chem. Phys. Lett. 218 (1994) 67.
- [20] K. Misawa, H. Ono, K. Minoshima, T. Kobayashi, Appl. Phys. Lett. 63 (1993) 577.
- [21] T. Kobayashi, T. Saito, H. Ohtani, Nature 414 (2001) 531.
- [22] H. Kano, T. Kobayashi, J. Phys. Chem. 116 (2002) 184.
- [23] A. Shirakawa, I. Sakane, M. Takasaka, T. Kobayashi, Appl. Phys. Lett. 74 (1999) 2268.
- [24] A. Baltuška, T. Fuji, T. Kobayashi, Opt. Lett. 27 (2002) 306.
- [25] N. Ishii, E. Tokunaga, T. Kobayashi, Phys. Rev. B (in press).
- [26] D.L. Akins, J.W. Macklin, J. Phys. Chem. 93 (1989) 5999.
- [27] D.L. Akins, Y.H. Zhuang, H.-R. Zyu, J.Q. Liu, J. Phys. Chem. 98 (1994) 1068.
- [28] C. Guo, M. Aydin, H.-R. Zyu, D.L. Akins, J. Phys. Chem. B 106 (2002) 5447.
- [29] T. Kobayashi, M. Hirasawa, Y. Sakazaki, H. Hane, Chem. Phys. Lett. (in press).
- [30] H. Kano, T. Kobayashi, J. Lumin. 100 (2002) 269.
- [31] T. Kobayashi, Mol. Cryst. Liq. Cryst. 314 (1998) 1.